THE JOURNAL OF PHYSICAL CHEMISTRY Letters

pubs.acs.org/JPCL

Letter

Observation of Four-Fold Boron−Metal Bonds in $RhB(BO^-)$ and RhB

Ling Fung Cheung,[†] Teng-Teng Chen,[†] G. Stephen Kocheril, Wei-Jia Chen, Joseph Czekner, and Lai-Sheng Wang*

Cite This: J. Phys. Chem. Lett. 2020, 11, 659−663

Read Online

ACCESS | Metrics & More | Article Recommendations | Supporting Information

ABSTRACT: The maximum bond order between two main-group atoms was known to be three. However, it has been suggested recently that there is quadruple bonding in C_2 and analogous eight-valence electron species. While the quadruple bond in C_2 has aroused some debates, an interesting question is: are main-group elements capable of forming quadruple bonds? Here we use photoelectron spectroscopy and computational chemistry to probe the electronic structure and chemical bonding in RhB_2O^- and RhB^- and show that the boron atom engages in quadruple bonding with rhodium in $RhB(BO)^-$ and neutral RhB. The quadruple bonds consist of two π-bonds formed between the Rh $4d_{xz}/4d_{yz}$ and B $2p_x/2p_y$ orbitals and two σ-bonds between the Rh $4d_{z^2}$ and B $2s/2p_z$ orbitals. To confirm the quadruple bond in RhB, we also investigate the linear $Rh{\equiv}B{-}H^+$ species and find a triple bond between Rh and B, which has a longer bond length, lower stretching frequency, and smaller bond dissociation energy in comparison with that of the Rh≡B quadruple bond in RhB.

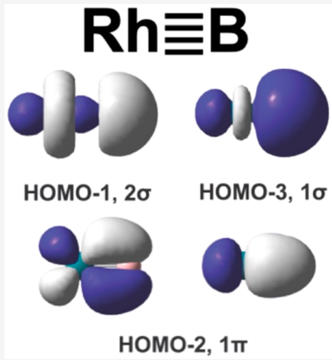

Ever since Lewis's epochal work on chemical bonds,[1] the maximum bond order between two main-group atoms has been known to be three. A quadruple bond between two Re atoms was first discovered in $[Re_2X_8]^{2-}$ type compounds,[2] while five-fold bonding was realized between two Cr(I) centers.[3] The maximum bond order between two atoms is now known to be six between two group-VIB atoms (Cr_2, Mo_2, W_2) based on theoretical analyses.[4] Recently, the idea of quadruple bonding between two main-group atoms has been suggested in C_2 and analogous eight-valence electron species on the basis of high-level theoretical analyses.[5] Further theoretical studies also indicated that carbon is involved in quadruple bonding with uranium in the linear triatomic CUO molecule,[6] as well as in terminal transition metal carbides.[7] However, the quadruple bond in C_2 has aroused some debates,[8−13] primarily due to the fact that the putative CC quadruple bond strength in C_2 is weaker than that in the classical HC≡CH triple bond in terms of bond lengths and force constants. Boron is electron-deficient and favors delocalized bonding in boranes and finite-sized clusters.[14−18] Localized boron−boron triple bonds are possible if electron-donor ligands are used. Boron−boron triple bonds were first observed in isolated molecules with CO and BO^- ligands[19,20] and synthesized with bulky carbene ligands.[21,22] Although many compounds containing metal−boron double bonds (borylenes) were known,[23] a metal−boron triple bond was found only recently in the $Bi{\equiv}B{-}BO^-$ molecule both experimentally and theoretically.[24] In searching for similar triple-bonded $M{\equiv}B{-}BO^-$ molecules with transition metal elements, we have examined RhB_2O^-. Surprisingly, we found that it does not have the expected linear $Rh{\equiv}B{-}BO^-$ structure. Rather, its most stable structure is found to be bent with the BO^- ligand coordinated to the Rh atom and a very short terminal Rh−B bond. Subsequently, we have investigated the diatomic RhB^- molecule and found that it has an even shorter Rh−B bond. Both experimental and theoretical analyses reveal that the B atom engages in quadruple bonding with Rh in RhB and $RhB(BO^-)$.

We did the experiments using two separate photoelectron spectroscopy (PES) apparatuses (see the SI for more experimental details). Briefly, the RhB^- and RhB_2O^- species were produced by laser vaporization of a Rh/^{11}B/Bi mixed target. The RhB_2O^- cluster was formed from the trace amount of oxide impurity on the target surface. The anionic clusters were extracted and analyzed using a time-of-flight mass spectrometer. The cluster of interest was mass-selected before being photodetached by a second laser. The photoelectron kinetic energies were measured with either a magnetic bottle time-of-flight analyzer[18,25] or a photoelectron imaging (PEI) system.[26] Figure 1 shows the photoelectron images and spectra of RhB^- at three photon energies using the PEI apparatus. Peak X represents the transition from the ground state of RhB^- to that of RhB, yielding the electron affinity (EA) of neutral RhB to be 0.961 eV. Short vibrational progression was observed for the ground-state transition with a vibrational frequency of 994 cm^{-1}. Peaks A at 1.339 eV and B at 1.428 eV are intense transitions, followed by a weak peak C at 1.525 eV. Although the separations between peaks A, B, and C are

Received: November 25, 2019
Accepted: January 8, 2020
Published: January 8, 2020

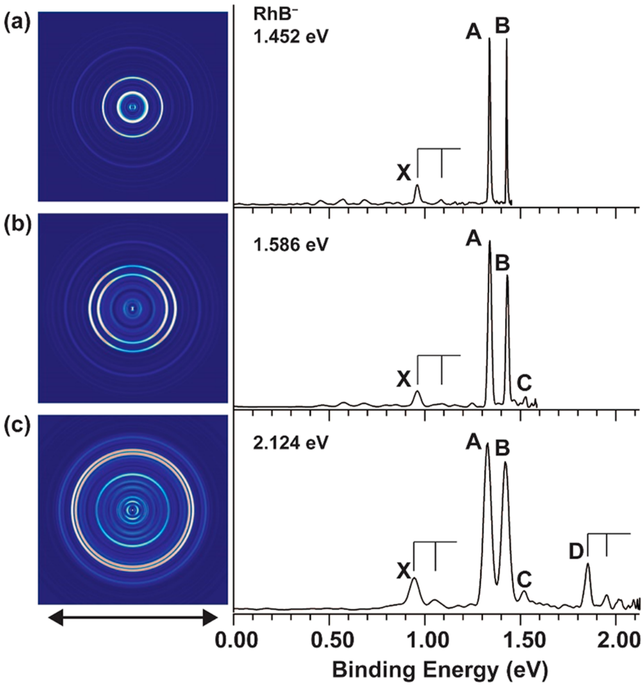

Figure 1. Photoelectron images and spectra for RhB^- at three photon energies, (a) 1.452, (b) 1.586, and (c) 2.124 eV. The vertical lines represent vibrational structures, and the double arrow below the images indicates the laser polarization.

roughly even, their relative intensities suggest that they do not represent a vibrational progression. Peak D has a binding energy of 1.852 eV with a short vibrational progression and a vibrational frequency of 789 cm^{-1}.

The photoelectron spectrum of RhB_2O^- displayed in Figure 2 was taken on the magnetic bottle PES apparatus at 193 nm.[18,25] The lowest binding energy band X corresponds to the detachment transition from the ground state of RhB_2O^- to that of neutral RhB_2O, whereas the higher binding energy bands (A–F) indicate detachment transitions to excited states of neutral RhB_2O. Band X yielded the first vertical detachment energy (VDE) of 2.66 eV and an adiabatic detachment energy (ADE) of 2.53 eV evaluated from its onset, which also represents the EA of neutral RhB_2O. A weaker band A was observed at a VDE of 3.59 eV, followed by a more intense band B at 3.91 eV. A broad band C was observed at around 4.95 eV, closely followed by a sharp feature D at 5.20 eV. The signal-to-noise ratios were poor above 5.5 eV, beyond which

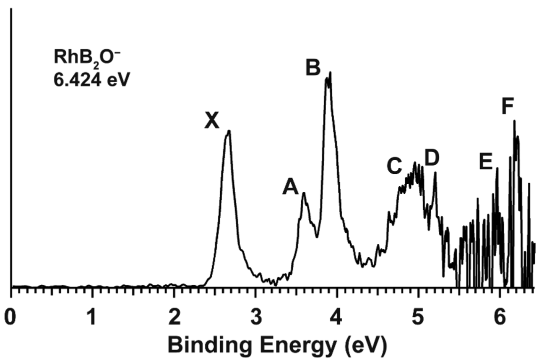

Figure 2. Photoelectron spectrum of RhB_2O^- at 193 nm (6.424 eV).

band E at ~6.0 eV and band F at ~6.2 eV were tentatively identified. The photoelectron spectra of RhB^- and RhB_2O^- serve as electronic fingerprints to allow analyses of their structures and bonding by comparison with theoretical calculations. The observed PES features and their binding energies are compared with the theoretical results in Tables S1 and S2 for RhB^- and RhB_2O^-, respectively.

The calculated structures for RhB^- and RhB_2O^- and their corresponding neutrals are shown in Figure 3 (see the SI for the theoretical details). The bond lengths of RhB and RhB^- were calculated at various levels of theory, which all predicted similar values between Rh and B, 1.703–1.712 Å for RhB^- and 1.685–1.689 Å for RhB (Table S3). The neutral Rh–B bond length agrees well with a previous experimental value (1.692 Å) obtained from optical spectroscopy,[27] as well as a previous theoretical calculation (1.698 Å).[28] Different structures were computed for RhB_2O^-. Surprisingly, the global minimum of RhB_2O^- was found to be bent (C_s, $^1A'$), consisting of a BO^- unit coordinated to the Rh atom (Figure 3b). The expected linear structure was found to be higher in energy by 0.60 eV (Figure S1a). The calculated Rh–B bond length between Rh and the BO unit was 1.996 Å, while that between Rh and the terminal B was 1.747 Å in the bent global minimum. There was a huge bond angle change between the BO unit and the RhB unit upon electron detachment, reducing from 99.8° in the anion to 80.4° in the neutral (Figure 3b). The Rh–BO bond length was also slightly shortened, and that between Rh and the terminal B was slightly lengthened in the neutral.

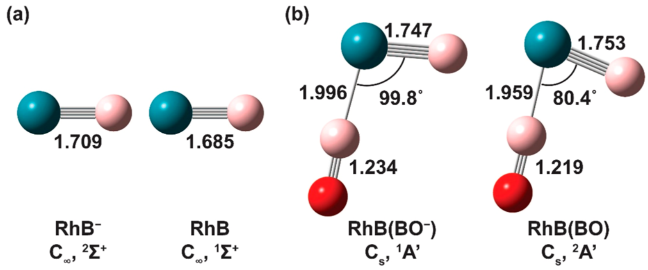

Figure 3. Calculated geometries and their ground electronic states, (a) RhB^- and RhB and (b) $RhB(BO^-)$ and RhB(BO).

The Kohn–Sham molecular orbitals (MOs) for RhB and the global minimum $RhB(BO^-)$ bent structure are given in Figure S2. There is similarity between the MOs related to the terminal RhB unit in $RhB(BO^-)$ and the bare RhB, as shown in Figure 4. A MO diagram for RhB, along with the atomic orbital compositions, is shown in Figure 5. The LUMO (3σ) of RhB, where the extra electron in the RhB^- anion resides, is a weakly antibonding orbital between the Rh 5s5p and the B 2s2p orbitals. The increased bond length and reduced vibrational frequency in the anion compared to those of the neutral are consistent with the weak antibonding character of the LUMO (Figure 3 and Table S1). The calculated electron detachment energy from the LUMO is 0.968 eV, in excellent agreement with the experimental value of 0.961 eV. The HOMO (1δ) of RhB consists of two degenerate nonbonding Rh $4d_{x^2-y^2}$ and $4d_{xy}$ orbitals. Electron detachment from the fully occupied 1δ MO can produce a triplet ($^3\Delta$) and singlet ($^1\Delta$) final state. Spin–orbit coupling will split the $^3\Delta$ state into three closely spaced states, $^3\Delta_{3,2,1}$, consistent with the observed peaks A, B, C (Table S1). The computed VDE of 1.445 eV for the $^3\Delta$ state is in excellent agreement with the average of the three spin–

https://dx.doi.org/10.1021/acs.jpclett.9b03484
J. Phys. Chem. Lett. 2020, 11, 659–663

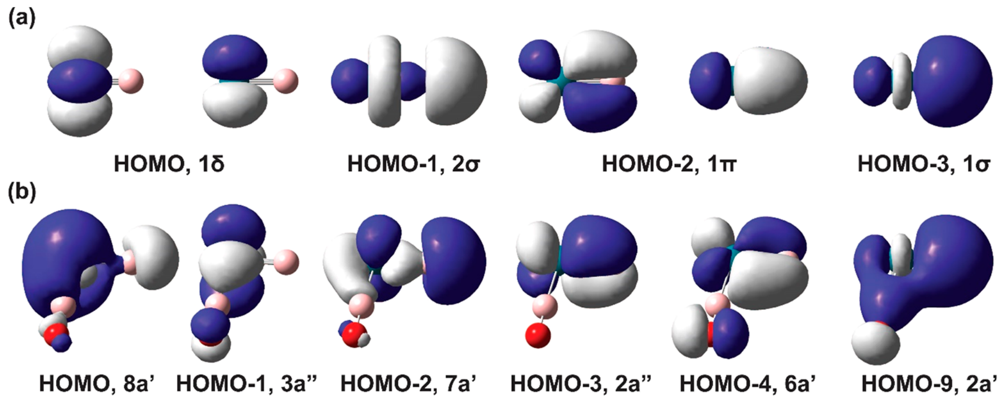

Figure 4. Valence MOs of RhB and the corresponding RhB-related orbitals in RhB(BO^-). (a) Valence MOs of RhB. (b) Corresponding MOs in RhB$(BO)^-$.

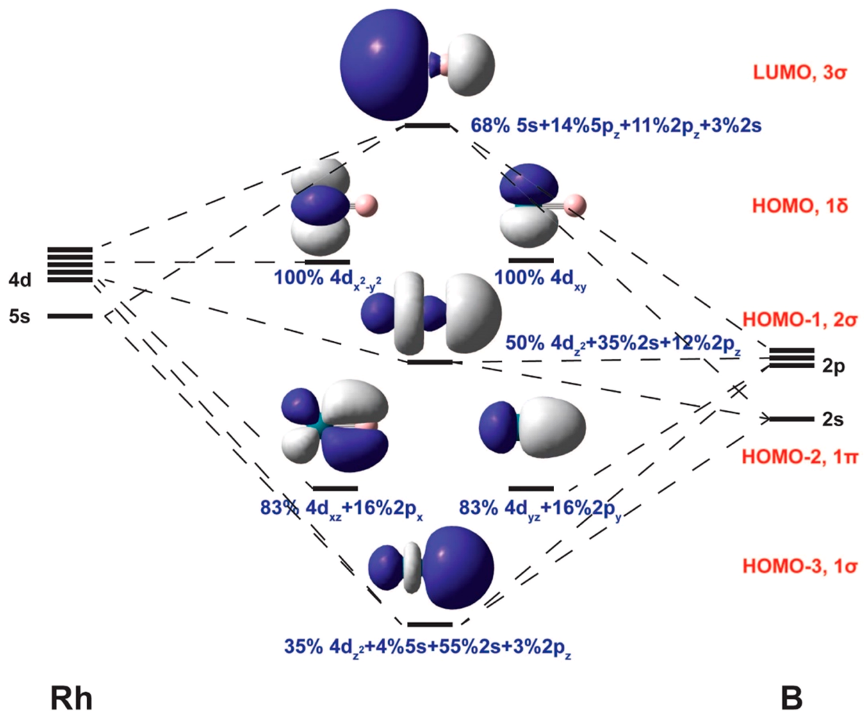

Figure 5. MO diagram and MO atomic compositions for RhB.

orbit components (Table S1). Furthermore, no vibrational progression is observed, consistent with the nonbonding nature of the 1δ MO. The computed VDE for the corresponding $^1\Delta$ final state is 2.140 eV, which is somewhat higher than the observed value. In addition, a short vibrational progression is observed for the $^1\Delta$ state, suggesting possible vibronic coupling of the $^1\Delta$ state with other nearby electronic states. The remaining four valence MOs are bonding orbitals between the Rh 4d_{z^2}/4d_{xz}/4d_{yz} and B 2s/2p_x/2p_y/2p_z orbitals.

The structure of RhB(BO^-) is basically a BO^- ligand coordinated to the RhB unit, as revealed in the MOs (Figure S2b). The HOMO, HOMO−1 to HOMO−4, and HOMO−9 correspond to the RhB unit, as compared with those of the bare RhB in Figure 4. The remaining five valence MOs (HOMO−5 to HOMO−8 and HOMO−10) belong to the BO^- ligand. The HOMO of RhB(BO^-), corresponding to one of the 1δ MOs in RhB, is involved in bonding interactions with the BO^- ligand. The calculated VDEs are in good agreement with the experimental data, as shown in Table S2 and Figure S3a. The calculated VDEs for the linear RhB−BO^- structure completely disagree with the observed spectrum (Figure S3b). A high-resolution PEI experiment was done for the X band, but a very congested spectrum was obtained (Figure S4a). This confirms the large geometry change between the RhB(BO^-) anion and its corresponding neutral, as borne out in the Franck−Condon simulation (Figure S4b).

The unusual bent structure of RhB(BO^-) with a short Rh−B bond prompted us to investigate the bonding in RhB. The computed Rh−B bond length of 1.685 Å is much shorter than the Rh≡B triple bond length using Pyykko's self-consistent Rh and B atomic covalent radii,[29] which give a triple bond length of 1.79 Å. Our computed Rh−B bond length agrees well with the previous experimental value of 1.692 Å and the previous theoretical value of 1.698 Å.[27,28] The MOs of Rh−B reveal four bonding orbitals (1σ, 1π, and 2σ) and two nonbonding orbitals (Figure 5). The extremely short Rh−B bond length is consistent with a quadruple bond between Rh and B (Rh≣B). The RhB bonding was considered to be a triple

https://dx.doi.org/10.1021/acs.jpclett.9b03484
J. Phys. Chem. Lett. 2020, 11, 659−663

bond previously because the 1σ MO was classified essentially as a 2s lone pair.[27,28,30] However, the bonding nature of the 1σ MO can be glimpsed by the fact that the bent Rh≣B(BO^-) structure is more stable than the linear Rh≡B−BO^- isomer, in which the B atom can form only a triple bond with Rh. The bonding of the two structures is compared in Figure S5 using the Adaptive Natural Density Partitioning (AdNDP) analyses.[31] It can be seen readily that four Rh−B bonds exist in the bent Rh≣B(BO^-) global minimum with two 4d lone pairs, whereas there are three Rh−B bonds and three 4d lone pairs in the linear Rh≡B−BO^- higher-energy isomer. The 1π MOs comprise the two π bonds. The 2σ MO consists of significant bonding interactions between the $4d_{z^2}$ orbital of Rh and the sp_z hybridized orbital of B, as shown more clearly in Figure 6 at a smaller isovalue. This bonding orbital was called a "doughnut" σ bond previously.[32,33]

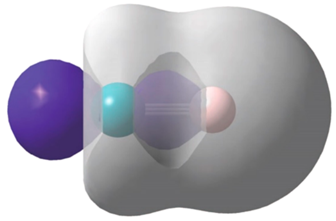

Figure 6. HOMO−1 (2σ) of RhB at isovalue = 0.020 e/bohr^3.

While this manuscript was being prepared, a similar quadruple bonding pattern between boron and iron was suggested in the $BFe(CO)_3^-$ complex.[34] On the other hand, it is noteworthy that the diatomic FeB was reported to have a quartet ground state and its bond length was calculated to be 1.73−1.77 Å,[35,36] which is significantly longer than the quadruple bond length reported in the $BFe(CO)_3^-$ complex (1.61 Å).[34] The carbonyl groups coordinating to the Fe atom are responsible for the short B−Fe bond. The current study reports the observation of quadruple bonding solely between a Rh atom and a B atom, the first diatomic molecule with a quadruple bond involving a boron atom.

To further confirm the bonding nature of the 1σ MO in RhB, we investigated the closed-shell $RhBH^+$ species, which can have only a Rh≡B triple bond (Figure S6). The computed Rh−B bond length is increased from 1.685 to1.747 Å, whereas the computed Rh−B stretching frequency is reduced from 956 to 826 cm^{-1} in comparison to those in the Rh≣B quadruple bond. We also computed the bond dissociation energies of Rh≣B [RhB ($^1\Sigma^+$) → Rh + B] and Rh≡B−H^+ [$RhBH^+$ ($^1\Sigma^+$) → Rh^+ + BH], as shown in Table 1. For each species, two reference states were used. The first entry in Table 1 for each species describes dissociation to the two products in their ground electronic states. Our computed value of 508 kJ/mol for RhB is in excellent agreement with a recent experimental measurement of 506.7 kJ/mol.[30] The second entry for each species in Table 1 describe dissociation to the products in their states that are ready to form the respective multiple bonds, i.e., Rh in its $4d^9$ (^2D) configuration for Rh≣B and BH in its $\sigma_{sp}{}^1\pi^1$ ($^3\Pi$) configuration for Rh≡BH^+. The latter should be more relevant to the intrinsic bond strength. In either case, the Rh≣B quadruple bond is significantly stronger than the Rh≡BH^+ triple bond. Therefore, unlike the putative quadruple bond in C_2, which has a longer bond distance and smaller stretching frequency than those in the C≡C triple bond in HC≡CH,[12] the Rh≣B quadruple bond is found to be significantly stronger than the Rh≡B triple bond in terms of a shorter bond length, higher vibrational frequency, and a larger bond energy. We also performed an energy decomposition analysis for RhB to understand the contributions of different orbitals to the bonding. The results shown in Table S4 reveal similar bonding contributions from the σ and π orbitals. Hence, we have both experimental and theoretical evidence for the existence of a Rh≣B quadruple bond in both the diatomic RhB and the RhB(BO^-) complex.

Table 1. Comparison of the Quadruple Bond Energy in Rh≣B and the Triple Rh≡B Bond Energy in $RhBH^{+a}$

species		reference states	ΔE (kJ/mol)
Rh≣B ($^1\Sigma^+$)	→	Rh ($5s^14d^8$, ^4F) + B ($2s^22p^1$, ^2P)	508
	→	Rh ($5s^04d^9$, ^2D) + B ($2s^22p^1$, ^2P)	543
Rh≡BH^+ ($^1\Sigma^+$)	→	Rh^+ ($5s^04d^8$, ^3F) + BH ($^1\Sigma^+$)	402
	→	Rh^+ ($5s^04d^8$, ^3F) + BH ($^3\Pi$)	529

[a]The calculations were done at the CCSD(T)/B/aug-cc-pVQZ/Rh/aug-cc-pVQZ-pp level of theory.

■ ASSOCIATED CONTENT

Supporting Information

The Supporting Information is available free of charge at https://pubs.acs.org/doi/10.1021/acs.jpclett.9b03484.

Detailed descriptions of the experimental and theoretical methods; experimental VDEs and their assignments by comparison with theoretical data; calculated Rh−B bond lengths at different levels of theory; energy decomposition analysis for RhB; structure and bonding of the linear RhB−BO^- isomer; MO analyses for RhB and $RhB(BO)^-$; comparison between experimental and theoretical data for the two isomers of RhB_2O^-; Franck−Condon simulation for $RhB(BO)^-$; AdNDP bonding analyses for the two isomers of RhB_2O^-; and structure and bonding of Rh−BH^+ (PDF)

■ AUTHOR INFORMATION

Corresponding Author

Lai-Sheng Wang − *Brown University, Providence, Rhode Island;* orcid.org/0000-0003-1816-5738; Email: lai-sheng_wang@brown.edu

Other Authors

Ling Fung Cheung − *Brown University, Providence, Rhode Island*

Teng-Teng Chen − *Brown University, Providence, Rhode Island*

G. Stephen Kocheril − *Brown University, Providence, Rhode Island*

Wei-Jia Chen − *Brown University, Providence, Rhode Island*

Joseph Czekner − *Brown University, Providence, Rhode Island;* orcid.org/0000-0002-7013-8334

Complete contact information is available at: https://pubs.acs.org/10.1021/acs.jpclett.9b03484

Author Contributions

†L.F.C. and T.-T.C. contributed equally to this work.

Notes

The authors declare no competing financial interest.

■ ACKNOWLEDGMENTS

This work was supported by the National Science Foundation (CHE-1763380).

■ REFERENCES

(1) Lewis, G. N. The Atom and the Molecule. *J. Am. Chem. Soc.* **1916**, *38*, 762−785.
(2) Cotton, F. A. Metal-Metal Bonding in $[Re_2X_8]^{2-}$ Ions and Other Metal Atom Clusters. *Inorg. Chem.* **1965**, *4*, 334−336.
(3) Nguyen, T.; Sutton, A. D.; Brynda, M.; Fettinger, J. C.; Long, G. J.; Power, P. P. Synthesis of a Stable Compound with Fivefold Bonding Between Two Chromium(I) Centers. *Science* **2005**, *310*, 844−847.
(4) Roos, B. O.; Borin, A. C.; Gagliardi, L. Reaching the Maximum Multiplicity of the Covalent Chemical Bond. *Angew. Chem., Int. Ed.* **2007**, *46*, 1469−1472.
(5) Shaik, S.; Danovich, D.; Wu, W.; Su, P.; Rzepa, H. S.; Hiberty, P. C. Quadruple Bonding in C_2 and Analogous Eight-Valence Electron Species. *Nat. Chem.* **2012**, *4*, 195−200.
(6) Hu, H. S.; Qiu, Y. H.; Xiong, X. G.; Schwarz, W. H. E.; Li, J. On the Maximum Bond Multiplicity of Carbon: Unusual C≣U Quadruple Bonding in Molecular CUO. *Chem. Sci.* **2012**, *3*, 2786−2796.
(7) Qiu, Y. H.; Hu, H. S.; Chen, G.; Li, J. Quadruple Bonding of Carbon in Terminal Carbides. *Sci. China: Chem.* **2014**, *57*, 426−434.
(8) Shaik, S.; Rzepa, H. S.; Hoffmann, R. One Molecule, Two Atoms, Three Views, Four Bonds? *Angew. Chem., Int. Ed.* **2013**, *52*, 3020−3033.
(9) Xu, L. T.; Dunning, T. H. Insights into the Perplexing Nature of the Bonding in C_2 From Generalized Valence Bond Calculations. *J. Chem. Theory Comput.* **2014**, *10*, 195−201.
(10) Danovich, D.; Hiberty, P. C.; Wu, W.; Rzepa, H. S.; Shaik, S. The Nature of the Fourth Bond in the Ground State of C_2: TheQuadruple Bond Conundrum. *Chem. - Eur. J.* **2014**, *20*, 6220−6232.
(11) Shaik, S.; Danovich, D.; Braida, B.; Hiberty, P. C. The Quadruple Bonding in C_2 Reproduces the Properties of the Molecule. *Chem. - Eur. J.* **2016**, *22*, 4116−4128.
(12) Hermann, M.; Frenking, G. The Chemical Bond in C_2. *Chem. - Eur. J.* **2016**, *22*, 4100−4108.
(13) de Sousa, D. W. O.; Nascimento, M. A. C. Is There a Quadruple Bond in C_2? *J. Chem. Theory Comput.* **2016**, *12*, 2234−2241.
(14) Lipscomb, W. N. The Boranes and Their Relatives. *Science* **1977**, *196*, 1047−1055.
(15) Zhai, H. J.; Alexandrova, A. N.; Birch, K. A.; Boldyrev, A. I.; Wang, L. S. Hepta- and Octacoordinated Boron in Molecular Wheels of Eight- and Nine-Atom Boron Clusters: Observation and Confirmation. *Angew. Chem., Int. Ed.* **2003**, *42*, 6004−6008.
(16) Zhai, H. J.; Kiran, B.; Li, J.; Wang, L. S. Hydrocarbon Analogs of Boron Clusters: Planarity, Aromaticity, and Antiaromaticity. *Nat. Mater.* **2003**, *2*, 827−833.
(17) Sergeeva, A. P.; Popov, I. A.; Piazza, Z. A.; Li, W. L.; Romanescu, C.; Wang, L. S.; Boldyrev, A. I. Understanding Boron through Size-Selected Clusters: Structure, Chemical Bonding, and Fluxionality. *Acc. Chem. Res.* **2014**, *47*, 1349−1358.
(18) Wang, L. S. Photoelectron Spectroscopy of Size-Selected Boron Clusters: From Planar Structures to Borophenes and Borospherenes. *Int. Rev. Phys. Chem.* **2016**, *35*, 69−142.
(19) Zhou, M.; Tsumori, N.; Li, Z.; Fan, K.; Andrews, L.; Xu, Q. OCBBCO: ANeutral Molecule with Some Boron-Boron Triple Bond Character. *J. Am. Chem. Soc.* **2002**, *124*, 12936−12937.
(20) Li, S. D.; Zhai, H. J.; Wang, L. S. $B_2(BO)_2^{2-}$— Diboronyl Diborene: ALinear Molecule with a Triple Boron-Boron Bond. *J. Am. Chem. Soc.* **2008**, *130*, 2573−2579.
(21) Braunschweig, H.; Dewhurst, R. D.; Hammond, K.; Mies, J.; Radacki, K.; Vargas, A. Ambient-Temperature Isolation of a Compound with a Boron-Boron Triple Bond. *Science* **2012**, *336*, 1420−1422.
(22) Arrowsmith, M.; Braunschweig, H.; Stennett, T. E. Formation and Reactivity of Electron-Precise B-B Single and Multiple Bonds. *Angew. Chem., Int. Ed.* **2017**, *56*, 96−115.
(23) Braunschweig, H.; Dewhurst, R. D.; Gessner, V. H. Transition Metal Borylene Complexes. *Chem. Soc. Rev.* **2013**, *42*, 3197−3208.
(24) Jian, T.; Cheung, L. F.; Chen, T. T.; Wang, L. S. Bismuth-Boron Multiple Bonding in BiB_2O^- and Bi_2B^-. *Angew. Chem., Int. Ed.* **2017**, *56*, 9551−9555.
(25) Wang, L. S.; Cheng, H. S.; Fan, J. Photoelectron Spectroscopy of Size-Selected Transition Metal Clusters: Fe_n^-, n = 3−24. *J. Chem. Phys.* **1995**, *102*, 9480−9493.
(26) León, I.; Yang, Z.; Liu, H. T.; Wang, L. S. The Design and Construction of a High−Resolution Velocity−Map Imaging Apparatus for Photoelectron Spectroscopy Studies of Size−Selected Clusters. *Rev. Sci. Instrum.* **2014**, *85*, 083106.
(27) Chowdhury, P. K.; Balfour, W. J. A Spectroscopic Study of the Rhodium Monoboride Molecule. *Mol. Phys.* **2007**, *105*, 1619−1624.
(28) Borin, A. C.; Gobbo, J. P. Low-Lying Singlet and Triplet Electronic States of RhB. *J. Phys. Chem. A* **2008**, *112*, 4394−4398.
(29) Pyykkö, P. Additive Covalent Radii for Single-, Double-, and Triple-Bonded Molecules and Tetrahedrally Bonded Crystals: ASummary. *J. Phys. Chem. A* **2015**, *119*, 2326−2337.
(30) Merriles, D. M.; Tieu, E.; Morse, M. D. Bond Dissociation Energies of FeB, CoB, NiB, RuB, RhB, OsB, IrB, and PtB. *J. Chem. Phys.* **2019**, *151*, 044302.
(31) Zubarev, D. Y.; Boldyrev, A. I. Developing Paradigms of Chemical Bonding: Adaptive Natural Density Partitioning. *Phys. Chem. Chem. Phys.* **2008**, *10*, 5207−5217.
(32) Patzschke, M.; Pyykko, P. Darmstadtiumcarbonyl and Carbide Resemble Platinum Carbonyl and Carbide. *Chem. Commun.* **2004**, *17*, 1982−1983.
(33) Hrobarik, P.; Straka, M.; Pyykko, P. Computational Study of Bonding Trends in the Metalloactinyl Series EThM and MThM'(E = N^-, O, F^+; M, M'=Ir^-, Pt, Au^+). *Chem. Phys. Lett.* **2006**, *431*, 6−12.
(34) Chi, C.; Wang, J. Q.; Hu, H. S.; Zhang, Y. Y.; Li, W. L.; Meng, L.; Luo, M.; Zhou, M.; Li, J. Quadruple Bonding between Iron and Boron in the $BFe(CO)_3^-$ Complex. *Nat. Commun.* **2019**, *10*, 4713.
(35) Tzeli, D.; Mavridis, A. Electronic Structure and Bonding of the 3d Transition Metal Borides, MB, M = Sc, Ti, V, Cr, Mn, Fe, Co, Ni, and Cu through All Electron Ab Initio Calculations. *J. Chem. Phys.* **2008**, *128*, 034309.
(36) Zhijian, W. Density Functional Study of 3d-Metal Monoborides. *J. Mol. Struct.: THEOCHEM* **2005**, *728*, 167−172.